MALAYSIAN JOURNAL OF ANALYTICAL SCIENCES

Published by The Malaysian Analytical Sciences Society

ISSN 1394 - 2506

HETEROEPITAXIAL GROWTH OF VACUUM-EVAPORATED Si-Ge FILMS ON NANOSTRUCTURED SILICON SUBSTRATES

(Pertumbuhan Epitaksi Filem Si-Ge Menggunakan Kaedah Evaporasi Vakum Diatas Silikon Berstruktur Nano)

Ayu Wazira Azhari[1,2]*, Kamaruzzaman Sopian[1], Saleem Hussain Zaidi[1]

[1]*Solar Energy Research Institute,*
Universiti Kebangsaan Malaysia, 43600 UKM Bangi, Selangor, Malaysia
[2]*School of Environmental Engineering,*
Universiti Malaysia Perlis, 01000 Kangar, Perlis, Malaysia

**Corresponding author: ayuwazira@unimap.edu.my*

Received: 8 February 2015 ; Accepted: 29 September 2015

Abstract

In this study, a low-cost vacuum-evaporated technique is used in the heteroepitaxial growth of Si-Ge films. Three different surface variations are employed: i.e. polished Si, Si micropyramids and Si nanopillars profiles. A simple metal-assisted chemical etching method is used to fabricate the Si nanopillars, with Ag acting as a catalyst. Following deposition, substrates are subjected to post-deposition thermal annealing at 1000°C to improve the crystallinity of the Ge layer. Optical and morphological studies of surface area are conducted using field emission scanning electron microscopy (FE-SEM), Energy Dispersive X-ray (EDX), Raman spectroscopy and infrared spectroscopy. From the infrared spectroscopy analysis, the energy bandgap for Si-Ge films is estimated to be around 0.94 eV. This high-quality Si-Ge film is most favourable for optics, optoelectronics and high-efficiency solar cell applications.

Keywords: heteroepitaxial growth, silicon germanium, thermal evaporation, nanostructured Si, metal assisted chemical etching

Abstrak

Dalam kajian ini, teknik evaporasi vakum berkos rendah digunakan dalam pertumbuhan epitaksi filem Si-Ge. Tiga variasi permukaan digunakan iaitu permukaan licin, permukaan berstruktur mikro-piramid dan permukaan berstruktur nano tiang. Satu kaedah berkos rendah berdasarkan kepada teknik punaran kimia terbantu logam (MACE) dengan perak (Ag) sebagai pemangkin telah dibangunkan untuk membentuk permukaan berstruktur nano. Selepas pemendapan, lapisan amorfus Ge kemudiannya menghablur di dalam relau penyepuhlindapan pada suhu 1000°C menghasilkan pertumbuhan epitaksi lapisan Ge dan Si-Ge. Lapisan Ge dan Si-Ge ini kemudiannya dicirikan menggunakan FESEM, EDX, spektroskopi Raman dan spektroskopi inframerah. Daripada pencirian analisi pektroskopi inframerah, julat jalur tenaga dianggarkan sekitar 0.94 eV. Filem Si-Ge berkualiti tinggi ini amat sesuai untuk aplikasi optik, opto-elektronik dan sel suria berkecekapan tinggi.

Kata kunci: pertumbuhan epitaksi, silicon germanium, evaporasi terma, Si berstruktur nano, punaran kimia terbantu logam

Introduction

Germanium was first discovered by Clemens Winkler in the year 1886 [1]. Back in 1947, J. Bardeen and W. Brattain had developed the first point contact transistor, followed by another discovery by W. Shockley a few months later [2,3]. However, since the first introduction of a Si transistor in 1954, Ge was immediately outshone, as Si was cheaper and available in large quantities [4]. It was not until 1980s that the full potentials of Si-Ge alloys

was finally revealed and they have regained a lot of interest since then [5,6]. Henceforth, this marked the beginning of extensive research into producing defect-free Si-Ge with wider application ranges, including for solar cells, optoelectronics, and fibre optic communications [7,8]. Rosenberg reported that in 2006, global consumptions of Ge included applications for polymerization catalysts (31%), fibre optics (24%), infrared optics (23%), electronics/solar cell applications (12%), and others (10%) [9].

Deposition of defect-free Ge on Si is highly desirable for several reasons. For instance, the realization of potential of using Ge as substrate for high-quality gallium arsenide (GaAs) growth has led to extensive studies in this area. This is also influenced by the slight lattice mismatch between Ge and GaAs, thus making it a promising substrate for *III-V* growth. Numerous studies show that Si-based Ge wafers are highly desirable in optoelectronics, laser diodes, and transistors, as well as high-efficiency solar cells [10]. Nevertheless, the growth of high-quality defect-free Ge wafers is a great challenge. As of today, Si is available in 12-inch diameter wafers and will soon reach 18-inch diameter in the near future. However, a 6-inch diameter Ge wafer is at least two orders of magnitude higher in cost and is believed to remain so for quite some time. It is believed that the growth of high-quality defect-free Ge on Si wafers will be able to reduce the cost.

The heteroepitaxial growth of Si-Ge is not an easy process as there is a lattice mismatch of about 4.2% between Si (lattice constant of 0.543 nm) and Ge (lattice constant of 0.566 nm), which leads to the formation of defects; i.e. misfit and threading dislocation. Misfit dislocations happen when there is a missing or dangling bond in the lattice between two layers of materials with different lattice constant. Hence, every misfit leads to the formation of a threading dislocation, where stress is terminated at the surface producing material of poor quality. Apart from that, deposition of Ge is limited to a certain thickness, whereby defects occur when deposition is done beyond the critical thickness. Matthews and Blakeslee discovered a simple yet practical model for determining the critical thickness [11]. This model has been used extensively in various studies involving the heteroepitaxial growth of Si-Ge layers [12].

Several methods have been developed to help reduce these defects, which include growth on graded layers [13], deposition using low temperature methods [14-16], point defects techniques [17], and growth on pattern substrates [18,19]. A recent study by Vanamu et al. on the growth of high-quality Ge films on pattern substrates demonstrated a significant reduction in dislocation density to about 5×10^{-5} cm^{-2} [20,21]. Nonetheless, there are some limitations to this approach that include the use of expensive plasma and a deep reactive io- etching process for the fabrication of pattern substrates. Furthermore, deposition of Ge was done using a chemical vapour deposition (CVD) process, which is well known to be costly and toxic.

This paper highlights the fabrication process of high-quality Si-Ge films on nanostructured Si wafers. A simple and low-cost metal-assisted chemical etching (MACE) method was chosen to prepare the well-ordered Si nanopillars (SiNPs), and the growth of Ge was conducted using a vacuum thermal evaporation technique. A recent study by Sorianello et al. demonstrated success in the deposition of crystalline Ge films using this inexpensive and low temperature deposition technique [22]. In order to grow epitaxial films, a-Ge films deposited on the Si surfaces were subjected to post-deposition thermal annealing in an N_2 ambient oven. A study by Chen et al. demonstrated that thermal annealing was able to improve the crystallinity, as well as the conductivity of Si-Ge layers [23]. The selection of annealing temperature range was based on similar work reported in various literature. Apart from that, the effects of post-deposition thermal annealing on the morphological and optical properties of the structure have also been studied. Si-Ge compositions are characterized with the aid of field emission scanning electron microscopy (FE-SEM), Energy Dispersive X-ray (EDX), Raman spectroscopy and infrared (IR) spectroscopy. For comparison purposes, deposition was also carried out on polished and micropyramid structures.

Materials and Methods

This study was divided into three main sections: the synthesis of Si nanopillar structures; the deposition of Ge using thermal evaporation technique; and the characterization of the whole structure. The first step comprises the synthesis of Si nanopillars to serve as templates for Ge heteroepitaxial growth. A simple yet effective method, known as metal-assisted chemical etching (MACE), was selected, with Ag as the metal catalyst in order to synthesize high aspect ration, nanopillar patterns. Heteroepitaxial growth of Ge films was then initiated by means of

depositing amorphous films through a thermal evaporation technique. In order to establish a baseline comparison, two sets of samples representing micropyramids profiles and polished Si profiles were also used as substrates, alongside the nanopillars' Si surfaces. The crystallization of the a-Ge films was then undertaken by thermal annealing. Characterizations of the produced structures were finally carried out using high-resolution FE-SEM, EDX, Raman spectroscopy and IR spectroscopy analysis.

Synthesis of Si Nanopillars

A MACE technique was employed to grow the nanometer (nm)-scale structures on *p*-type (100) Si wafers (1–10 Ω.cm, boron doped), with silver (Ag) acting as a catalyst. Prior to deposition, the 5" Si wafers went through damage removal in a boiling solution of 10% NaOH for 15 minutes and cleaning was done in a solution containing HF/HNO_3 for 10 minutes, followed by immersion in diluted HF for 1 minute. A two-step etching process was used in which Ag was first deposited on the wafers in a mixture of $AgNO_3/HF$ solution, at various etchant concentrations and time. This was followed by etching with Ag as the mask in a solution of HF/H_2O_2 at various time intervals. Both deposition and etching were carried out at room temperature, in order to maintain the etching rate. Once etching was completed, the wafers were dipped in diluted HNO_3 followed by immersion in diluted HF to remove any Ag residues and oxide layers coating the SiNPs.

Thermal Evaporation of Ge Films

For the purpose of this study, Si wafers of different surface morphologies were used in order to determine the effect of various surface structures in the deposition process. Three different surface variations were chosen, representing SiNPs (Ag etched), Si micropyramids (IPA-KOH etched) and polished Si. Figure 1 depicts the cross-sectional view of SiNPs (Figure 1a), Si micropyramids (Figure 1b) and polished Si profiles (Figure 1c).

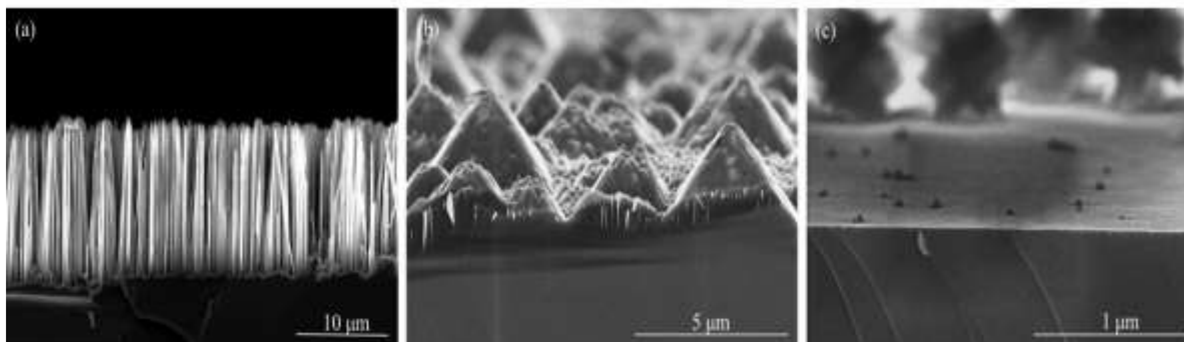

Figure 1. Cross-sectional view of (a) Si nanopillars (b) Si micropyramids and (c) polished Si profiles

All structured and polished Si wafers were diced into 3 cm × 3 cm size using a YMS-50D laser scribing machine. Prior to deposition, the Si wafers were cleaned in a standard cleaning solution. For this application, Ge was deposited using a thermal evaporation method in an HHV Auto 306 coater, at vacuum pressure of 5.3×10^{-5} Torr and filament current in the 6–7A range, for time intervals varying from 5 to 10 seconds. Ge targets of 99.999% purity (obtained from a commercial source), ranging from 100 to 1500 mgs, were used for deposition, resulting in varying thickness of Ge layers. The Ge content was determined by EDX analysis and a surface morphological study was carried out using a Hitachi S8000 ultra-high-resolution FE-SEM.

Thermal Annealing and Characterization of Ge Films

To further improve the quality of the Si-Ge alloys, the wafers were subjected further to thermal annealing in a N_2 flow annealing chamber at 1000°C for 30 minutes, where recrystallization of Ge took place. Structural analyses of the samples were performed using FE-SEM, and the optical properties of the deposited Ge films were determined using Raman spectroscopy. The Infra-red spectrum was observed with the use of a simple monochromator, as shown in Figure 2. Light from a halogen lamp passed through the monochromator and was reflected at different

angles for different wavelengths by a grating inside the monochromator. By rotating the grating it was possible to tune the wavelength of transmitted light through the exit slit of the monochromator.

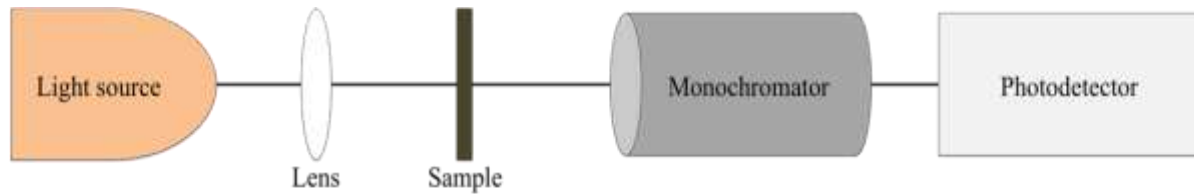

Figure 2. Optical setup for IR spectroscopy measurement

Results and Discussion

Synthesis of Si Nanopillars

Figure 3 shows a cross-sectional view of the SEM images of SiNP arrays at various etchant concentrations and etching times. It can be clearly seen that the length of the SiNPs increased with etching time, as shown in Figure 3(a) and (b) ,where the etching time was increased from 30 minutes to 40 minutes, respectively. However, when the concentration of H_2O_2 was increased from 0.1 M to 0.55 M, the lateral etching at the tips of the pillars was also increased, which eventually destroyed the top surface of the pillars, resulting in the formation of a thinner wafer with shorter SiNPs fabricated at the same time intervals, as can be seen in Figure 3 (c) and (d). These results are in agreement with those reported in [24,25].

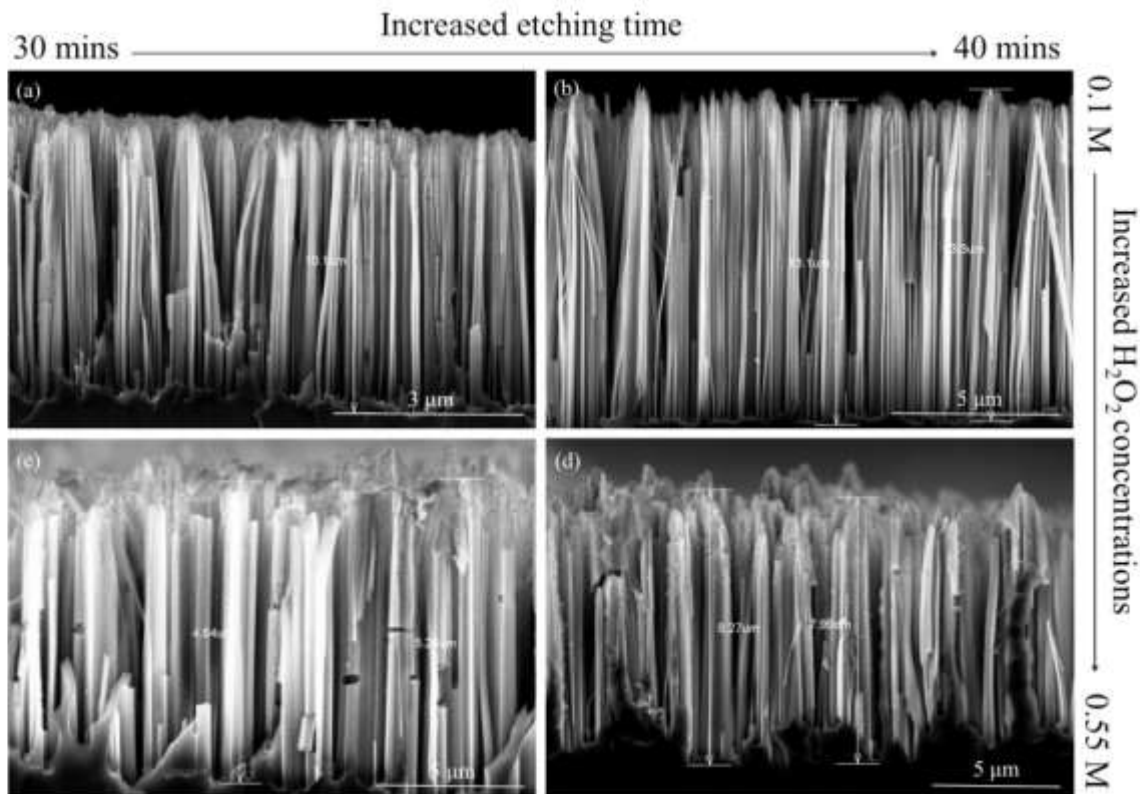

Figure 3. SEM images of SiNW arrays at various etchant concentrations and etching time

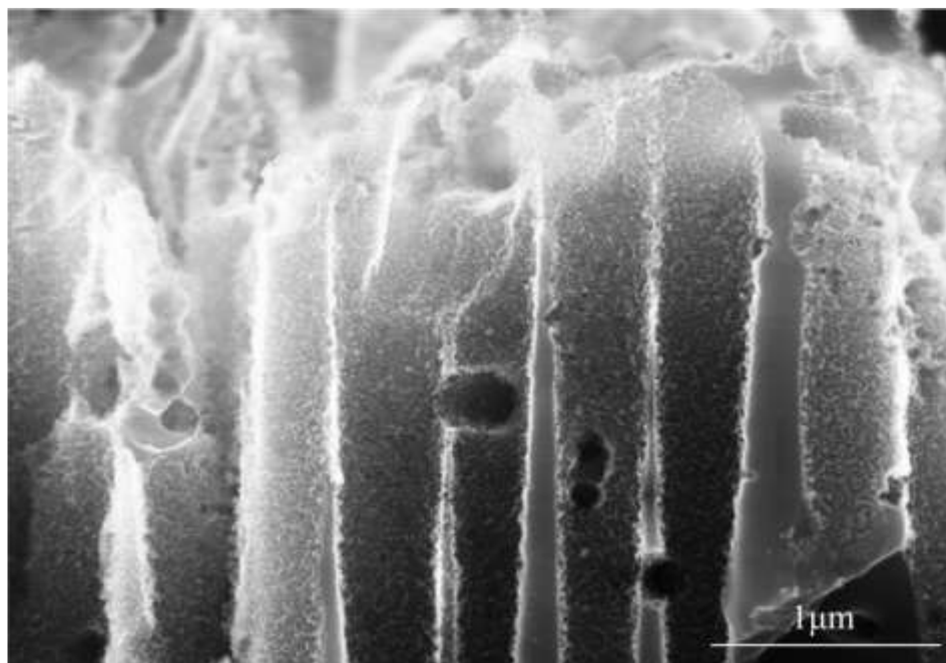

Figure 4. High magnification FE-SEM image of surface morphology of Si nanopillars. Etching was conducted in 0.55 M H_2O_2 for 40 minutes

Closer inspection on the surface morphology of the Si structures depicted rough surfaces with dense and homogeneous meso-porous layers on the sidewalls, in a region a few nm from the surface, as indicated in Figure 4. In fact, most studies reported the formation of these meso-porous layers while etching with HF/H_2O_2 [26,27]. The existence of H_2O_2 promotes the nucleation of Ag into nano-size particles at the top surface of the structures that leads to the formation of meso-pores. A higher concentration of H_2O_2 induces more nucleation of micro- and nano-sized Ag particles on top of the structures. Parallel and lateral etching of these micro and nano Ag particles produce micro- and meso-pores that lead to the formation of porous silicon instead of nm-scale pillars.

It is believed that the meso-porous layer formed on the sidewalls of the pillars is a result of the presence of loose Ag^+ as a result of the reaction of Ag particles with peroxide from H_2O_2 [26]. These Ag^+ re-nucleate and form Ag nanoparticles that etch laterally into the structures, forming meso-pores on the sidewalls of the structures [28]. A study by Li et al. [29] also suggests that the formation of a meso-pore layer on the sidewalls of these structures is greatly affected by the doping levels of the wafers. It is believed that higher doping levels produce rougher surfaces as compared to lower doping levels of the wafers [29]. This could be seen in a study reported by Qu et al. [30], where etching was conducted on four different doping levels; 1–5 Ω.cm, 0.3–0.8 Ω.cm, 0.008–0.016 Ω.cm and 0.001–0.002 Ω.cm. Results from this study clearly show that the porosity of the Si nanopillars increases as the doping levels decreases [30].

Optical Characterization of Si Nanopillars

The total reflectance and transmittance spectra were measured using a Perkin Elmer Lambda 750 UV-Vis-NIR spectrophotometer in a wavelength range of 400 to 2000 nm. From the reflectance and transmittance value, the absorption coefficient was calculated. The data plotted in Fig. 3 for etched samples exhibits significantly low reflection, in comparison to polished Si reflectance values of 1% and 20 % which have been observed for Si wafers with nanopillars and micropyramids structures, respectively. Huang et al. reported similar results, where the reflectivity of Si structures reduced from porous structures to nanopillars with the lowest reflectivity reported for pillars with the greatest length [18]. Apart from that, the reflectance values reduced to almost 0% in the far-infrared region for both nanopillars and micropyramid structures. In comparison, the average reflectance and absorption (as

shown in Figure 5) for polished Si were 50% and 0%, respectively. SiNPs' surfaces are known to exhibit low reflectance values of less than 1%, which also makes them a candidate to replace AR films in solar cells. This is proven by a high absorption of almost 90% compared to polished Si.

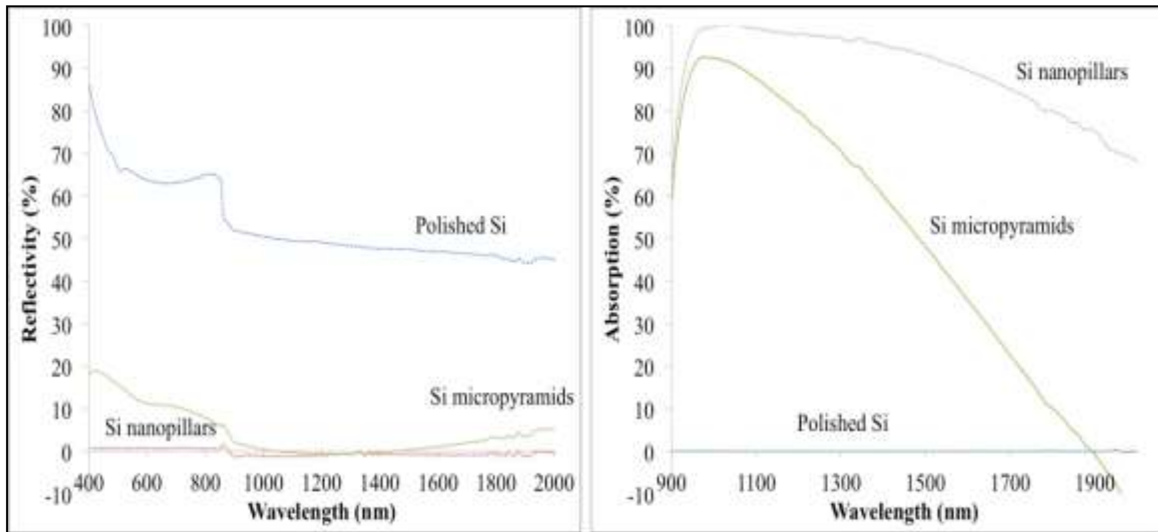

Figure 5. Optical reflectance and absorption for three different surface structures

Raman spectra (Figure 6) of both polished Si and SiNPs show a typical narrow peak at 520 cm^{-1} indicating high crystallinity of both polished Si and SiNPs wafers. This also means that after etching, the SiNPs maintain the same crystalline structure as the polished Si.

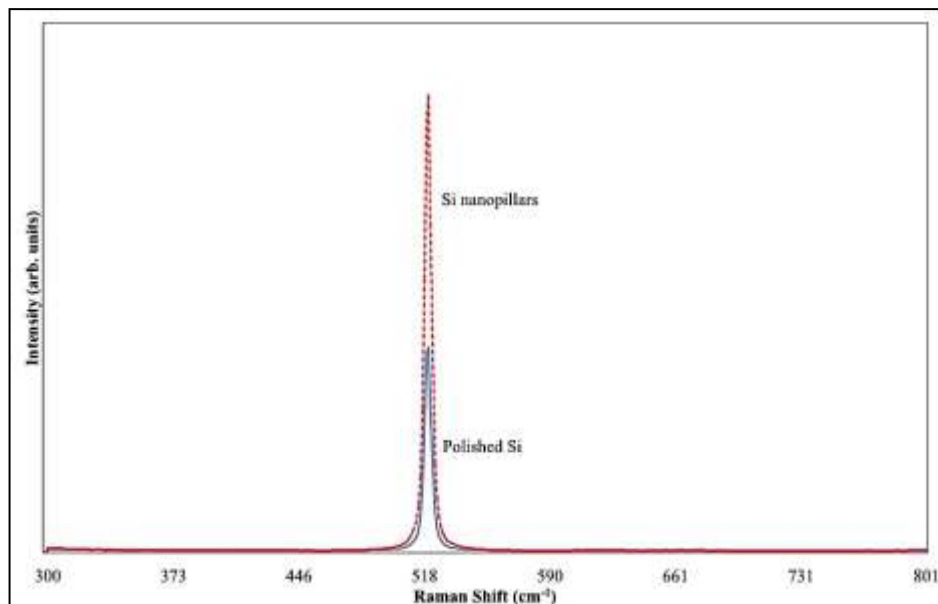

Figure 6. Raman spectra of polished and nanostructured Si

Thermal Evaporation of Ge Films

Visual inspections show that a high Ge content (by weight) deposited on polished Si wafers resulted in the formation of Ge flakes on the surface. However, a smooth layer of Ge with acceptable uniformity presents when deposited on structured Si surfaces. This proves that the deposition of Ge on a polished surface beyond the critical thickness results in defects; in this case, it becomes flaky. In contrast, when deposited on structured surfaces, defects are not visible and a smooth surface is acquired.

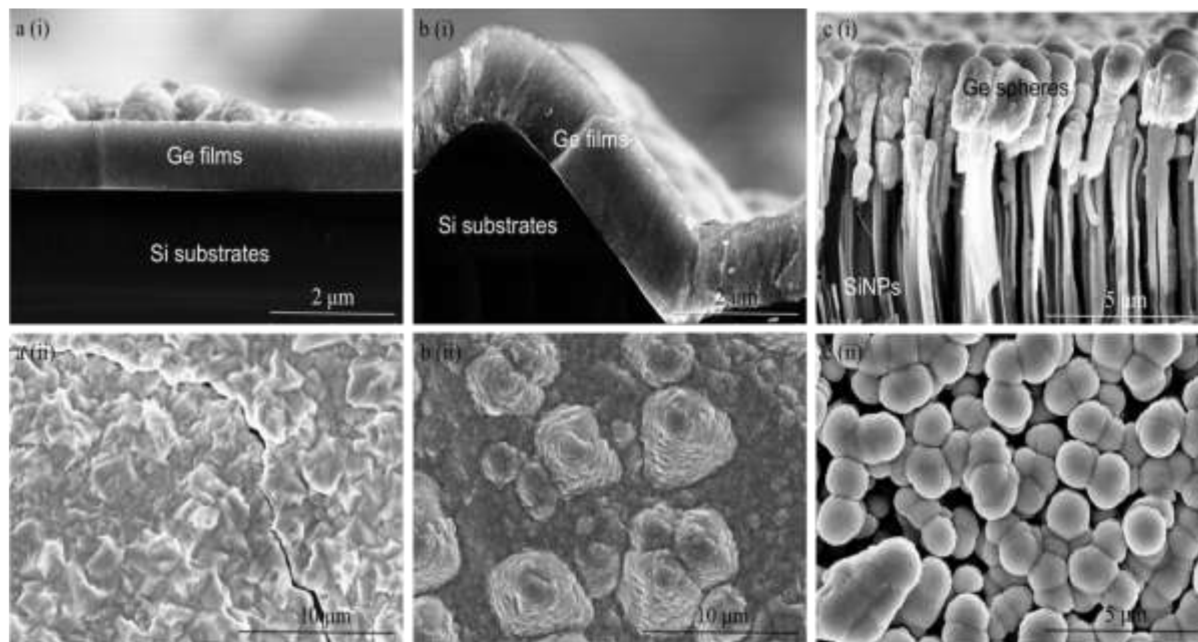

Figure 7. FESEM images of (i) cross-sectional and (ii) top views of Ge deposited on (a) polished Si. (b) Si micropyramids and (c) Si nanopillars

FE-SEM is used to determine the morphology and thickness of the as-deposited Ge layers. Figure 7 shows the thickness and morphology of Ge deposited on three different surface structures. Ge is deposited on polished Si to serve as a baseline, and assisted in determining the thickness of the Ge layers. At 1000 mgs Ge (by weight), the thickness of the Ge layer deposited on polished Si is about 980 nm (Figure 7a (i)). Apparently, deposition of a Ge layer with a thickness beyond 1 μm is quite impossible on a flat surface as it can cause dislocations and defects. This is indicated by the formation of flakes during the deposition of Ge. FE-SEM images also showed these defects, as can be seen by the formation of cracks, as shown in Figure 7a (ii). It is well known that defects occur owing to the 4.2% lattice mismatch between the Ge and Si substrates. The lattice mismatch induces strain within the layers and this strain increases with increasing film thickness. When the strain finally relaxes, dislocation occurs, resulting in the formation of cracks at the interface [11,12,31].

In contrast, the deposition on structured Si wafers reveals the opposite. Imprints of the underlying Si structures are replicated on the surface of these structured wafers, as reflected in Figs. 6 b (ii) and c (ii). Deposition of Ge on Si micropyramids' surface results in the formation of a well-distributed layer of Ge of about 1.5 μm on top of the pyramid structures, as indicated in Figure 7b (i). No formation of flakes was noticed during deposition and cracks are not visible from the FE-SEM images (Figure 7b (ii)). On the other hand, the deposition of Ge on SiNPs surfaces reveals the accumulation of Ge around the tips of the SiNPs, resulting in clustering of Ge spheres on the surface. Cracks are also not visible from the FE-SEM images for deposition on SiNPs profiles, as shown in Figure 7c (ii). These prove that depositions of Ge on structured surfaces reduce dislocations and defects, thus improving the

overall quality of Ge layers. However, these Ge layers are believed to be in either metastable or stable condition, in accordance to Matthews' and Blakeslee's model [11].

In this study, the structured surfaces eventually act as pseudomorphic layers. These virtual layers provide dislocation sites at the interface between Si substrates and the pseudomorphic layer, thus relaxation takes place and reduces the defect density [32]. Various studies reveal the same effects, where growth of Ge on virtual substrates is able to reduce defects and dislocation density to less than ~10^5 cm^{-2} [15,18,33]. Vanamu et al. [20,21] indicate that the quality of heteroepitaxial layers improved with decreasing the patterned sizes of the pseudomorphic layers [20,21].

Thermal Annealing and Characterization of Ge Films

A study by Chen et al. [23] shows that thermal annealing is able to improve the crystallinity as well as the conductivity of Si-Ge layers [23]. Figure 8a (i) and (ii) depict the top and cross-sectional views of a polished Si profile after being subjected to thermal annealing. It is believed that Ge flakes melt and agglomerate, forming randomly oriented crystalline trenches at the surface. As expected, major and minor cracks present due to dislocations and defects. This, however, is already predicted, as Ge layers deposited on polished Si are already in a relaxed condition and annealing only makes things worse.

On the other hand, annealing of Ge deposited on structured surfaces shows some significant outcomes. Ge deposited on Si micropyramids' structures results in the recrystallization and accumulation of Ge particles on the sidewalls of the pyramids, as shown in Figure 8b (i) and (ii). Surface inspection shows no replication of pyramid structures present, and is replaced by a considerably flat surface. This result is in accordance with a study by Abd Rahim et al. [34], where annealing of Ge deposited on polished Si beyond 800°C reduced the surface roughness, as compared to as-deposited samples [34]. Furthermore, minor cracks were visible, but no sign of major cracks existed. This shows that the Ge layer was previously in the metastable region of the Matthews and Blakeslee model,and annealing caused this layer to relax.

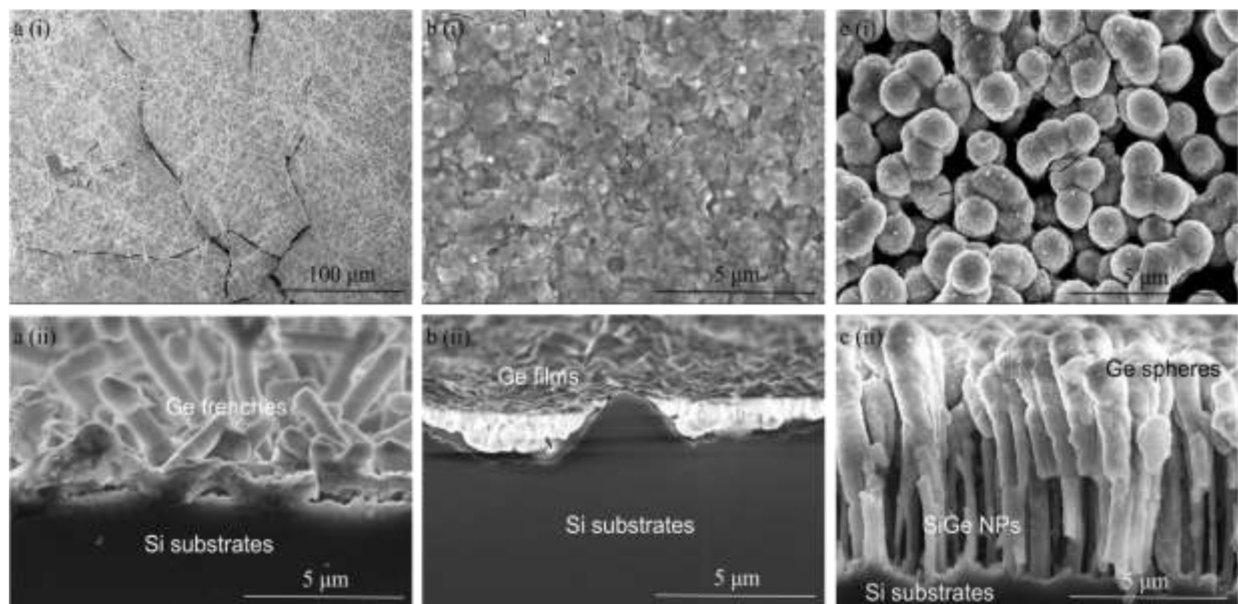

Figure 8. Surface and cross-sectional views of Ge deposited on (a) polished Si, (b) Si micropyramids and (c) Si nanopillars. Formations of cracks are visible for Ge deposited on polished Si and Si micropyramids.

As for the SiNPs profile, annealing causes Ge to melt and re-crystallize on the sidewalls of the pillars instead of accumulating at the tips. Cross-sectional views reveal poor coverage of Ge, where the areas in between the trenches are not completely filled (Figure 8 (ii)). It is also noticeable that the SiNPs profiles remain intact and coalescence or disintegration of the clustering Ge is not visible, even after being subjected to thermal annealing at 1000 ^{o}C. This may be attributed to the lack of uniformity and the broad width between the SiNPs arrays. The top view exhibits islands of clustered Ge with minor cracks present but at a reduced extent, as can be seen in Figure 8 c (i). This shows that the deposition of Ge on nanostructured surfaces improved the overall quality of the Ge layers. Studies by Vanamu et al. demonstrate the same results, where defects density is reduced for epitaxial growth of Ge/Si-Ge on nanostructured surfaces, as compared to deposition on micro-structured surfaces [19-21].

Further assessment using EDX shows the composition of Si and Ge of the samples. A high Ge concentration of up to 80% is noticed from the analysis of the sample before annealing, as seen in Figure 9 (*a*). Subsequently, the Ge content is reduced to about 60% after annealing with increases in O_2 (Figure 9 (*b*)). However, the percentage of Si does not differ as much, before and after being subjected to thermal annealing. This is in agreement with the FE-SEM micrograph images, where annealing causes Ge from the tips of the pillars to melt and agglomerate on the sidewalls of the pillars. It is also noticed that a high concentration of oxide presents after annealing that may be due to the process of annealing not conducted in a vacuum, which leads to the formation of the oxide layer.

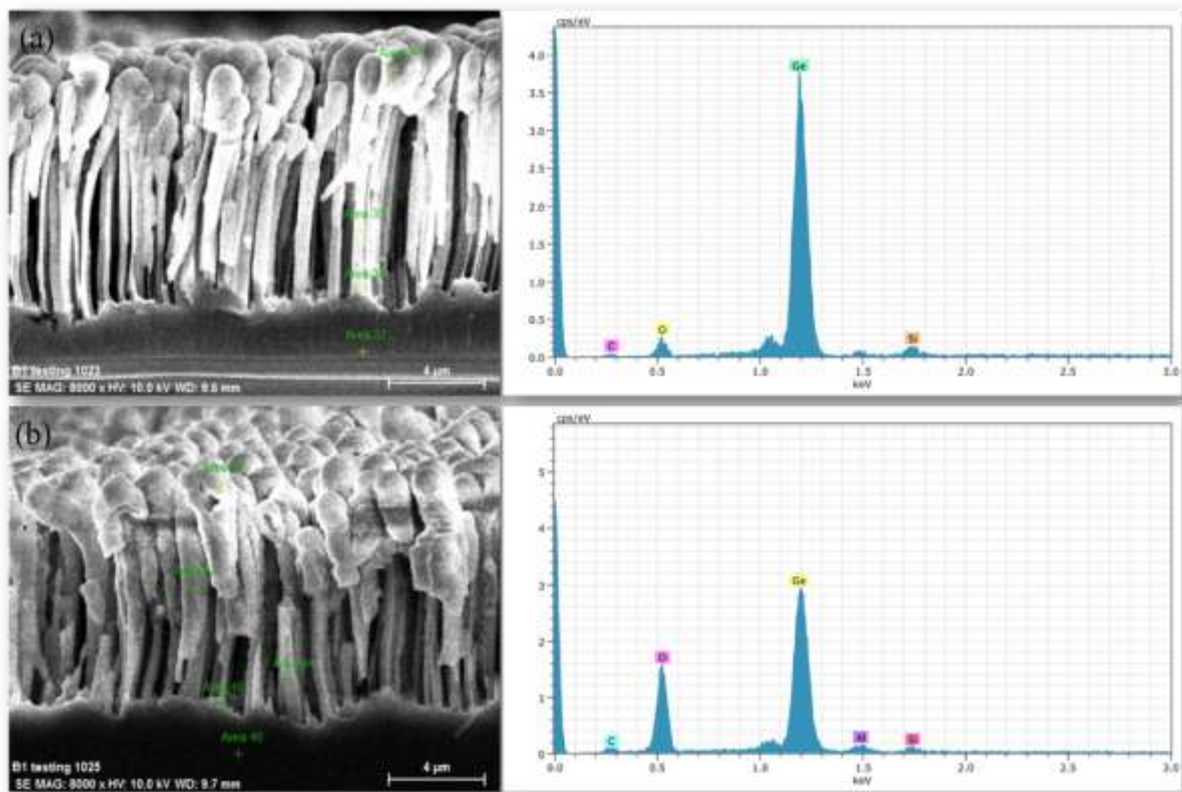

Figure 9. EDX analyses on composition of Si and Ge (*a*) before and (*b*) after annealing

In order to investigate the effect of thermal annealing on the crystallinity of Ge, Raman backscattered spectroscopy is measured on the as-deposited and annealed samples (Figure 10). Raman spectra of the as-deposited Ge show Ge-Ge peak at 280 cm^{-1}, the Si-Ge peak at 445 cm^{-1} and Si-Si peak at 520 cm^{-1} for SiNPs samples. However, Si-Si peaks for polished Si and Si micropyramids samples are absent. The broad and smooth band spectrum centred at 280 cm^{-1} resembled amorphous Ge structure [35,36]. After annealing at 1000°C, no significant spectral shift appeared for polished Si and Si micropyramid samples, which suggests a fully relaxed layer [37]. On the other hand, a slight hump, observed in the SiNPs sample at 300 cm^{-1}, marked the initial growth of Ge nano-crystals [34]. It is also observed that before annealing, Si-Ge peaks are hardly visible for all three samples. However, the spectrum shows a prominent peak at 445 cm^{-1} after being subjected to high temperature, suggesting some improvement in the crystallinity of Si-Ge structures.

In order to investigate the effect of thermal annealing on the crystallinity of Ge, Raman backscattered spectroscopy is measured on the as-deposited and annealed samples (Figure 10). Raman spectra of the as-deposited Ge show Ge-Ge peak at 280 cm^{-1}, the Si-Ge peak at 445 cm^{-1} and Si-Si peak at 520 cm^{-1} for SiNPs samples. However, Si-Si peaks for polished Si and Si micropyramids samples are absent. The broad and smooth band spectrum centred at 280 cm^{-1} resembled amorphous Ge structure [35,36]. After annealing at 1000°C, no significant spectral shift appeared for polished Si and Si micropyramid samples, which suggests a fully relaxed layer [37]. On the other hand, a slight hump, observed in the SiNPs sample at 300 cm^{-1}, marked the initial growth of Ge nano-crystals [34]. It is also observed that before annealing, Si-Ge peaks are hardly visible for all three samples. However, the spectrum shows a prominent peak at 445 cm^{-1} after being subjected to high temperature, suggesting some improvement in the crystallinity of Si-Ge structures.

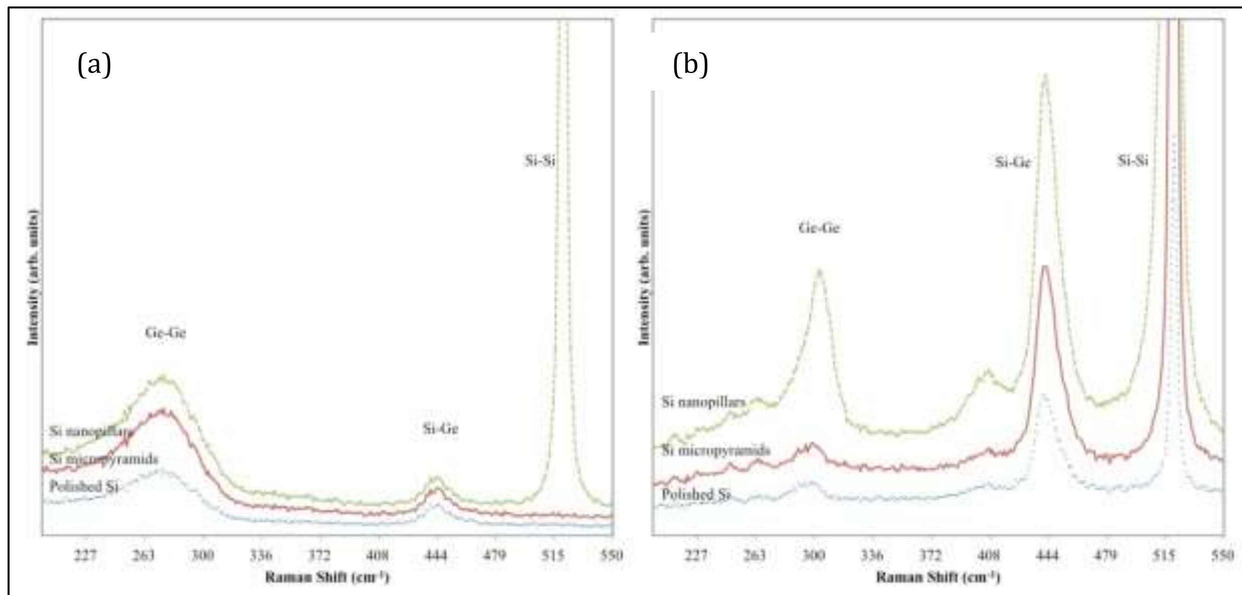

Figure 10. Raman spectra of (a) as-deposited and (b) annealed samples for different surface textured

The IR spectrum for three different surface profiles before and after annealing is plotted as a function of wavelength in Figure 11. Polished Si shows the highest transmission value followed by Si micropyramid profiles. On the other hand, deposition on SiNPs profiles shows the lowest transmission for both as-deposited and annealed samples. Annealing causes increments in the transmission value of about two magnitudes higher for both polished Si and the Si micropyramid structures and about three magnitudes higher for SiNPs profiles.

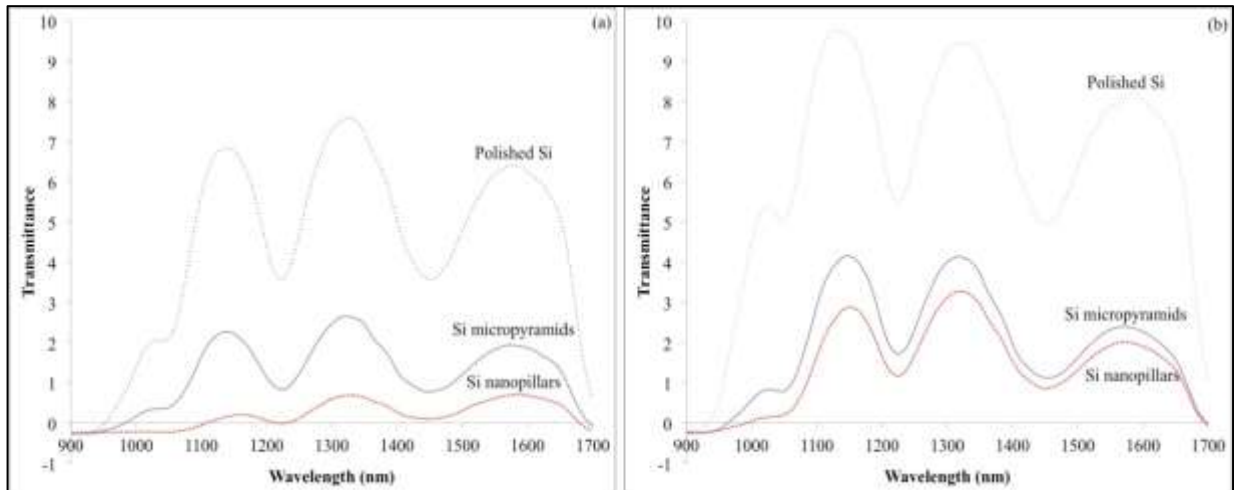

Figure 11. Infra-Red transmissions spectrum of three different surface structures (a) as-deposited and (b) annealed

Closer inspection of IR transmission measurements for SiNPs profiles revealed a slight shift before and after being subjected to thermal annealing (Figure 12). By assuming that the reflectivity is constant, the maximum transmittance and minimum absorbance are considered to be at the same wavelength. From this, it is possible to roughly estimate the bandgap energy (E_g) for both samples by using equation (1) below

$$E_g = \frac{hc}{\lambda_{max}} \quad (1)$$

where h is the Plank constant, c is the speed of light and λ_{max} is the maximum transmittance. From the calculation, the E_g for the as-deposited sample is estimated at around 0.93 eV, with a slight shift to 0.94 eV after being subjected to thermal annealing. The slight shift in the energy bandgap shows some changes in the lattice parameter of the Ge films. However, detail characterization using x-ray diffraction is needed to determine the lattice properties of these structures.

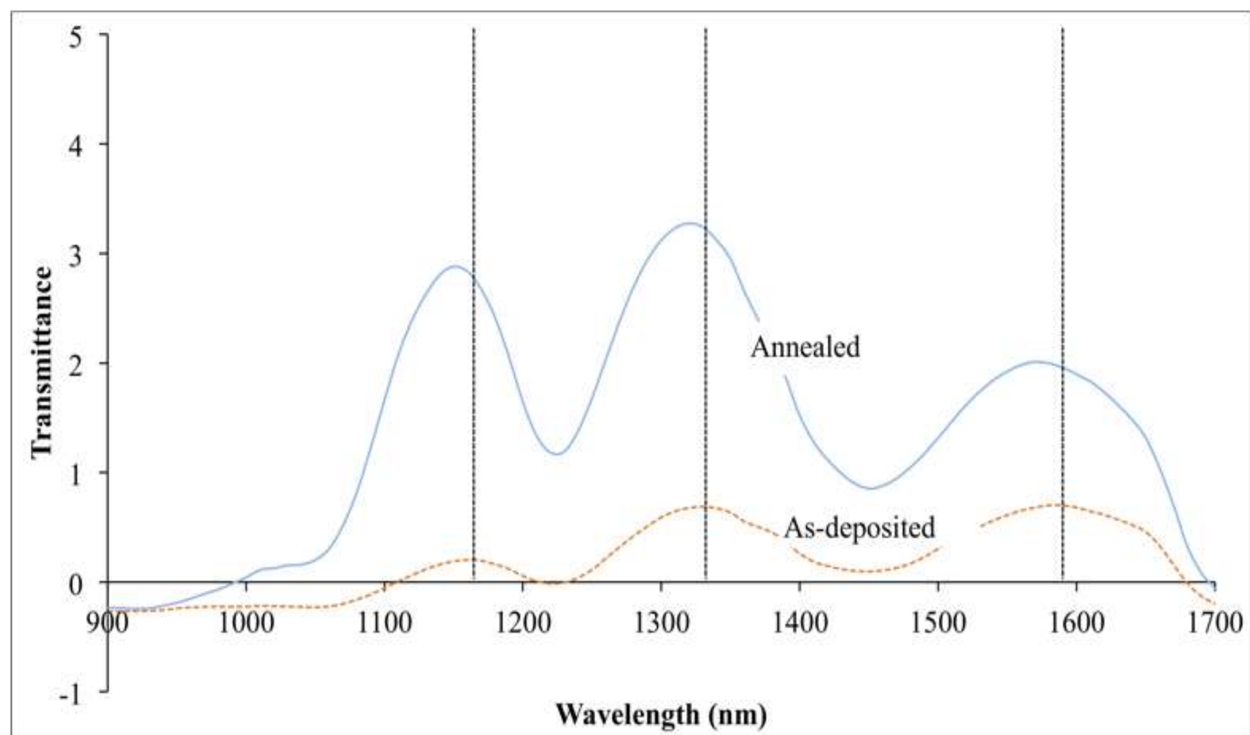

Figure 12. Infra-Red transmittance for nanopillars profiles before and after annealing

Conclusion

In conclusion, the deposition of Ge on nanostructured Si is proven to improve the overall quality in the heteroepitaxial growth of Si-Ge. However, optimization of SiNPs is needed in order to improve the overall quality of Si-Ge hetero-structures. This can be done by finding the most ideal pattern dimensions and producing more uniform and aligns arrays of SiNPs. It is believed that a pointed, needle-like tip is more favourable for the deposition of Ge rather than the current flat tip. This will eventually reduce the accumulation of Ge at the top of the pillars, thus producing total coverage and completely filling the trenches. Furthermore, pattern dimensions of the SiNPs should also be reduced to less than 100 nm in order to obtain the better deposition of Ge.

Acknowledgement

The authors would like to thank the Ministry of Education Malaysia for the financial support under the Long-term Research Grant Scheme (LRGS) and the SLAB/SLAI fellowship scheme. A million thanks also goes to SERI Colloquium 2014 for providing the platform to the discussion session and disseminate the findings.

References

1. Winkler, C. (1886). Germanium, Ge, ein neues, nichtmetallisches Element. *Berichte der deutschen chemischen Gesellschaft*, 19 (1): 210-211.
2. Brattain, W. H. and Bardeen, J. (1948). Nature of the forward current in germanium point contacts [15]. *Physical Review*, 74 (2): 231-232.
3. William F. Brinkman, Douglas E. Haggan and Troutman, W. W. (1997). A History of the Invention of the Transistor and Where It Will Lead Us. *IEEE Journal of Solid-state Circuits*, 32 (12): 1858 - 1865.
4. Depuydt, B., Theuwis, A. and Romandic, I. (2006). Germanium: From the first application of Czochralski crystal growth to large diameter dislocation-free wafers. *Materials Science in Semiconductor Processing*, 9: 437–443.

5. Schubert, M. B., Weller, H. C., Eberhardt, K. and Bauer, G. H. (1989). Structural Properties of a-Sil-xGex:H. *Journal of Non-Crystalline Solids*, (114): 528 - 530.
6. Yang, S.-H. and Lee, W.-J. (1985). Preparation of Hydrogenated Amorphous Germanium by Reactive Thermal Evaporation. *Solid State Communications*, 53 (11): 993-995.
7. Said, K., Poortmans, J., Caymax, M., Loo, R., Daami, A., Bremond, G., Kruger, O. and Kittlerc, M. (1999). High quality, relaxed SiGe epitaxial layers for solar cell application. *Thin Solid Films*, (337): 85-89.
8. Wang, C.-C., Liu, C.-Y., Lien, S.-Y., Weng, K.-W., Huang, J.-J., Chen, C.-F. and Wuu, D.-S. (2011). Hydrogenated amorphous silicon–germanium thin films with a narrow band gap for silicon-based solar cells. *Current Applied Physics,* 11 (1): S50-S53.
9. Rosenberg, E. (2009). Germanium: environmental occurrence, importance and speciation. *Review Environment Science and Biotechnology*, 8 (29–57): 29-57.
10. Vanamu, G., Datye, A. K., Dawson, R. and Zaidi, S. H. (2006). Growth of high-quality GaAs on Ge⁄Si[sub 1−x]Ge[sub x] on nanostructured silicon substrates. *Applied Physics Letters*, 88 (25): 251909.
11. Matthews, J. W. and Blakeslee, A. E. (1974). Defects in epitaxial multilayers: I. Misfit dislocations. *Journal of Crystal Growth*, 27: 118-125.
12. Kasper, E. (2008). Current topics of silicon germanium devices. *Applied Surface Science*, 254 (19): 6158-6161.
13. Fan, Q. H., Chen, C., Liao, X., Xiang, X., Zhang, S., Ingler, W., Adiga, N., Hu, Z., Cao, X. and Du, W. (2010). High efficiency silicon–germanium thin film solar cells using graded absorber layer. *Solar Energy Materials and Solar Cells*, 94 (7): 1300-1302.
14. Datta, S., Xu, Y., Mahan, A. H., Branz, H. M. and Cohen, J. D. (2006). Superior structural and electronic properties for amorphous silicon–germanium alloys deposited by a low temperature hot wire chemical vapor deposition process. *Journal of Non-Crystalline Solids*, 352 (9-20): 1250-1254.
15. Shah, V. A., Dobbie, A., Myronov, M. and Leadley, D. R. (2011). High quality relaxed Ge layers grown directly on a Si(001) substrate. *Solid-State Electronics*, 62 (1): 189-194.
16. Chen, C., Zhou, Z., Chen, Y., Li, C., Lai, H. and Chen, S. (2010). Thermal stability of SiGe films on an ultra thin Ge buffer layer on Si grown at low temperature. *Applied Surface Science*, 256 (22): 6936-6940.
17. Renrong, L., Jing, W. and Jun, X. (2009). Fabrication of High Quality SiGe Virtual Substrates by Combining Misfit Strain and Point Defect Techniques. *Tsinghua Science and Technology*, 14 (1): 62-67.
18. Gentile, P., Eymery, J., Leroy, F., Fournel, F., Meziere, J. and Perreaub, P. (2005). Germanium growth on nanopatterned surface studied by STM. *Journal of Crystal Growth* 275: 1609–1613.
19. Vanamu, G., Datye, A. K. and Zaidi, S. H. (2005). Growth of high quality Ge⁄Si[sub 1−x]Ge[sub x] on nano-scale patterned Si structures. *Journal of Vacuum Science & Technology B: Microelectronics and Nanometer Structures*. 23 (4): 1622.
20. Vanamu, G., Datye, A. K. and Zaidi, S. H. (2005). Heteroepitaxial growth on microscale patterned silicon structures. *Journal of Crystal Growth*, 280 (1-2): 66-74.
21. Vanamu, G., Datye, A. K. and Zaidi, S. H. (2006). Epitaxial growth of high-quality Ge films on nanostructured silicon substrates. *Applied Physics Letters*, 88 (20): 204104.
22. Sorianello, V., Colace, L., Assanto, G., Notargiacomo, A., Armani, N., Rossi, F. and Ferrari, C. (2011). Thermal evaporation of Ge on Si for near infrared detectors: Material and device characterization. *Microelectronic Engineering*, 88: 526–529.
23. Chen, Y.-H., Liu, J.-C., Chen, Y.-R., Lin, J.-W., Chen, C.-H., Lu, W.-H. and Li, C.-N. (2013). Enhancing performance of amorphous SiGe single junction solar cells by post-deposition thermal annealing. *Thin Solid Films*, 529: 7-9.
24. Chartier, C., Bastide, S. and Lévy-Clément, C. (2008). Metal-assisted chemical etching of silicon in HF–H2O2. *Electrochimica Acta*, 53 (17): 5509-5516.
25. Ashour, E. S. M., M.Y.Sulaiman, Amin, N. and Ibrahim, Z. (2012). Characterization of Si nanowires synthesized using metal-assisted wet-chemical etching. *Malaysian Journal of Fundamental & Applied Sciences*, 8 (3): 137 - 142.
26. Smith, Z. R., Smith, R. L. and Collins, S. D. (2013). Mechanism of nanowire formation in metal assisted chemical etching. *Electrochimica Acta*, 92: 139-147.
27. Tsujino, K. and Matsumura, M. (2007). Morphology of nanoholes formed in silicon by wet etching in solutions containing HF and H2O2 at different concentrations using silver nanoparticles as catalysts. *Electrochimica Acta*, 53 (1): 28-34.

28. Bai, F., Li, M., Song, D., Yu, H., Jiang, B. and Li, Y. (2012). One-step synthesis of lighly doped porous silicon nanowires in HF/AgNO3/H2O2 solution at room temperature. *Journal of Solid State Chemistry*, 196: 596-600.
29. Li, X. (2012). Metal assisted chemical etching for high aspect ratio nanostructures: A review of characteristics and applications in photovoltaics. *Current Opinion in Solid State and Materials Science*. 16 (2): 71-81.
30. Zhong, X., Qu, Y., Lin, Y.-C., Liao, L. and Duan, X. (2011). Unveiling the Formation Pathway of Single Crystalline Porous Silicon Nanowires. *ACS Applied Material Interfaces*, 3 (2): 261-270.
31. Kasper, E. (1996). Silicium germanium heterodevices. *Applied Surface Science*, 102 189-193.
32. Kasper, E. and Heim, S. (2004). Challenges of high Ge content silicon germanium structures. *Applied Surface Science*, 224 (1-4): 3-8.
33. Chen, P. S., Lee, S. W., Lee, M. H. and Liu, C. W. (2008). Formation of relaxed SiGe on the buffer consists of modified SiGe stacked layers by Si pre-intermixing. *Applied Surface Science*, 254 6076–6080.
34. Rahim, A. F. A., Hashim, M. R., Ali, N. K., Rusop, M., Ooi, M. D. J. and Yusoff, M. Z. M. (2013). Self-assembled Ge islands and nanocrystals by RF magnetron sputtering and rapid thermal processing: The role of annealing temperature. *Applied Surface Science*, 275 193-200.
35. Jadkar, S. R., Sali, J. V., Kshirsagar, S. T. and Takwale, M. G. (2002). Narrow band gap, high photosensitivity a-SiGe:H films prepared by hot wire chemical vapor deposition (HW-CVD) method. *Materials Letters*, 52: 399-403.
36. Soukup, R. J., Ianno, N. J., Darveau, S. A. and Exstrom, C. L. (2005). Thin films of a-SiGe:H with device quality properties prepared by a novel hollow cathode deposition technique. *Solar Energy Materials and Solar Cells* 87 (1-4): 87-98.
37. Coonan, B. P., Griffna, N., Beechinor, J. T., Murtagh, M., Redmond, G., Crean, G. M., HollaèNder, B., Mantl, S., Bozzo, S., Lazzari, J.-L., D'avitaya, F. A., Derrien, J. and Paul, D. J. (2000). Investigation of Si/SiGe heterostructure material using non-destructive optical techniques. *Thin Solid Films*, 364 75-79.